


---

This is the **accepted version** of the journal article:

Descals, Adrià; Gaveau, David L. A.; Verger, Aleixandre; [et al.]. «Unprecedented fire activity above the Arctic Circle linked to rising temperatures». *Science*, Vol. 378, Issue 6619 (November 2022), p. 532-537. DOI 10.1126/science.abn9768

---

This version is available at <https://ddd.uab.cat/record/288886>

under the terms of the  **IN** COPYRIGHT license

# Title: Unprecedented fire activity above the Arctic Circle linked to rising temperatures

Authors: Adrià Descals<sup>1,2\*</sup>, David L. A. Gaveau<sup>3</sup>, Aleixandre Verger<sup>1,2,4</sup>, Douglas Sheil<sup>5,6</sup>, Daisuke Naito<sup>6,7</sup>, Josep Peñuelas<sup>1,2</sup>

## Affiliations:

<sup>1</sup>CREAF, Centre de Recerca Ecològica i Aplicacions Forestals; Cerdanyola del Vallès, Barcelona 08193, Catalonia, Spain.

<sup>2</sup>CSIC, Global Ecology Unit CREAF-CSIC-UAB; Bellaterra, Barcelona 08193, Catalonia, Spain.

<sup>3</sup>TheTreeMap; Bagadou Bas, 46600 Martel, France.

<sup>4</sup>CIDE, CSIC-UV-GV; València 46113, Spain.

<sup>5</sup>Forest Ecology and Forest Management Group, Wageningen University and Research; P.O. Box 47, 6700 AA, Wageningen, the Netherlands.

<sup>6</sup>Center for International Forestry Research (CIFOR); P.O. Box 0113 BOCBD, Bogor 16000, Indonesia.

<sup>7</sup>Graduate School of Agriculture, Kyoto University; Kitashirakawaoiwake-cho, Sakyo-ku, Kyoto, 606-8502, Japan.

\*Corresponding author. Email: a.descals@creaf.uab.cat

**Abstract:** Arctic fires can release large amounts of carbon from permafrost peatlands. Satellite observations reveal that fires burned approximately 4.7 Mha in 2019 and 2020, accounting for 44% of the total burned area in the Siberian Arctic for the entire 1982-2020 period. The summer of 2020 was the warmest in four decades, with fires burning an unprecedentedly large area of carbon-rich soils. We show that factors of fire associated with temperature have increased in recent decades and identified an exponential relationship between these factors and annual burned area. Large fires in the Arctic are likely to recur with climatic warming before mid-century, because the temperature trend is reaching a threshold in which small increases in temperature are associated with exponential increases in the area burned.

**One-Sentence Summary:** Near-term climatic warming will result in an exponential increase in burned area in Arctic carbon-rich soils.

**Main Text:** Emissions from Arctic wildfires jeopardize global climate goals (1). The Arctic is warming rapidly due to a climate change related phenomenon known as “Arctic amplification” (2); annual mean temperature has already increased more than 2°C compared to the preindustrial era (3), and is expected to reach 3.3 to 10°C above the 1985-2014 average by 2100 (4). These increased temperatures result in thawing of permafrost and deterioration of peatlands with emissions of carbon dioxide and methane (5–7). High-latitude peatlands are expected to become a net carbon source as the consequence of global warming (8). The release of carbon creates positive feedback with additional emissions contributing to further warming and thawing with further peatland degradation and emissions. In this context, the numerous fires identified by satellite thermal sensors in Eastern Siberia in 2020 (9) raise particular concerns due to the resulting fire emissions (10).

Wildfires are common in the Arctic and Subarctic (11), but their size, frequency, and intensity are expected to increase as the climate warms (12). Extreme weather, such as that in 2020 in the Siberian Arctic (13), is expected to become more severe as Arctic oscillations weaken over time (14). Previous research in the Alaskan tundra suggests that the annual burned area might be two times higher than the 1950-2010 period by the end of the century as warmer and drier conditions coincide more frequently (15). The conditions that affected the Arctic fire seasons of 2019 and 2020 in the Siberian Arctic have provided new empirical observations between climatic factors and burn extent and may already be indicating the changes in fire regimes expected by the end of the century. The fire seasons of 2019 and 2020, however, raised two uncertainties. First, whether the annual burned area above the Arctic Circle was actually increasing. Satellite-derived burned-area products tend to underestimate the true extent of burning (12) and rigorous validation techniques are required (16). Second, even if the burned areas in 2019 and 2020 were the largest yet observed, the links to other trends required evaluation.

We assessed annual burned area in the Siberian Arctic (latitudes >66.5°N) for 1982-2020 using six satellite-derived maps of burned areas (Fig. S1). We investigated the Siberian Arctic because it is where most burning occurs above the Arctic Circle and fire frequency appeared to be increasing (9). We investigated ten factors associated with the likelihood of fire: six climatic variables (air and surface temperature, total precipitation, wind speed and direction, and vapor-pressure deficit (VPD)), three variables describing the vegetation conditions (length of the growing season, mean normalized difference vegetation index (NDVI<sub>mean</sub>), and climatic water deficit (CWD)), and the number of ignitions, a direct factor of fires. We evaluated how these factors have varied over the last four decades and their relationships with satellite-derived estimates of annual burned areas. Lastly, we investigated the future trends of annual burned area and fire emissions under future Representative Concentration Pathway (RCP).

## Results

### *Trends of burned area for 1982-2020*

Between 1982 and 2020, the satellite burned area products indicate that 12.97 Mha burned in the circumpolar region (latitudes > 66.5°N). The Siberian Arctic, a region with continuous permafrost, accounted for 71% of this burned area. The years 2019 and 2020 had the greatest mapped burned area in Siberia above the Arctic Circle (Fig. 1a) (see Supplementary Text A for consistency of the time series of the burned area and Fig. S2), which represents 44% of the total mapped burned area (9.24 Mha) in the region from 1982 to 2020. The burned area mapped in the Siberian Arctic varied between the satellite products, most notably the MCD64A1 product for

2019 and 2020 (Fig. 2a). The burned areas for 2020 were 1.71, 2.38, 2.59, and 2.62 Mha for MCD64A1, C3SBA10, Landsat, and Sentinel-2, respectively.

The sampling-based burned area in 2020, based on an assessment of errors of omission and commission (16), was nearly 3 Mha (MCD64A1 =  $2.83 \pm 0.26$  Mha, C3SBA10 =  $2.92 \pm 0.17$  Mha, Landsat =  $2.92 \pm 0.15$  Mha, and Sentinel-2 =  $2.99 \pm 0.14$  Mha) (see full assessment of accuracy in Table S1 and a description of the results in Supplementary Text B). The area estimate for 2019 and 2020 amounts to approximately 4.7 Mha. The mapped burned area is lower than the estimated burned area for all four products because the omission errors of the ‘burned’ class (ranging from 15.5% to 53.7%) are higher than the commission errors (ranging from 3.2% to 23.0%). Our estimates of carbon emissions from burning were 55.3 and 90.4 Tg C for 2019 and 2020, respectively, which is 156.7 and 256.1 Tg CO<sub>2</sub>-eq (including CO<sub>2</sub> and CH<sub>4</sub>) (Fig. S3). Fires in 2020 damaged a wide area (1.01 Mha) of carbon-rich peatlands (organic carbon storage >20 kg C m<sup>-2</sup>) indicated by a reference map of soil carbon storage (8) (Fig. 1b). The area of carbon-rich peatlands affected by fires has also recently expanded: 49% of total burned area occurred in these areas within the last eight years of the record, and 28% occurred in 2020 (Fig. 2b).

### ***Trends of the fire factors for 1982-2020***

Various factors that may exacerbate the risk of fire have increased significantly over the last four decades in the Siberian Arctic (Fig. 3 and Fig. S4). Air temperature, NDVI, the length of the growing season, and VPD have steadily risen. The average increase in summer air temperature was 0.66 °C/decade. In 2019 and 2020, the mean summer air temperature was 11.35 °C and 11.53 °C, which was 2.65 °C and 2.82 °C higher than the 1982–2020 average, respectively. CWD, a proxy of plant water stress defined as the difference between potential and actual evapotranspiration, also increased between 1982 and 2020, although the linear trend likely began in the 2000s. More surprisingly, however, was the abrupt increase in CWD in 2019 and 2020. The estimated number of ignitions, total precipitation, and wind speed all had strong interannual variations, and the slope of their trends was not significantly different to zero.

The annual number of detected ignitions was relatively consistent, with a median of 143, but high counts were observed in specific years, peaking at 423 in 2020. 72% of these 2020 ignitions were detected within 20 days, between June 13 and July 3, reaching Siberian Arctic regions as far north as 72.9° (Fig. S5). Interestingly, these ignitions coincided with anomalously high values of convective available potential energy (CAPE) (Fig. S6), an indicator of convective storms and lightning. Between June 13 and July 3, satellite thermal sensors registered a rapid increase in the number of active fire detections, which accounts for 40.6% of all hotspots detected in 2020. In contrast, hotspots detected before June 13 represented only 1.1%. Similar peaks in the number of detected ignitions, preceding high rates of active fire detection, occurred concurrently with high CAPE values in 2002, 2005, 2013, and 2018.

### ***Sensitivity of the burned area to the fire factors***

Linear and exponential regressions were used to analyze the best association between the annual burned area (aggregated with the median across available satellites for each year) and the factors of fire regime. An exponential regression was the best regression model (Fig. 4); the annual burned area increased exponentially when specific thresholds were exceeded. For example, the

four years with the largest mapped burned areas (2001, 2018, 2019, and 2020) had a mean summer air temperature  $>10^{\circ}\text{C}$ . The best fit was for CWD, which explained 92% of the interannual variability in the burned area. Other factors with a high  $R^2$  were summer air temperature (87%), VPD (77%), and number of ignitions (83%). The annual burned area was correlated most weakly with total precipitation (15.1%). We also detrended the fire factors using the linear regression shown in Fig. 3 before determining the correlation with the annual burned area to reduce the potential of spurious correlations. The detrended correlations (Fig. S7) confirmed the high  $R^2$  for CWD (91%), air temperature (80%), VPD (71%), and number of ignitions (80%), but the correlations decreased for  $\text{NDVI}_{\text{mean}}$  (from 78 to 11%) and length of season (from 34 to 7%).

We further examined the potential relationships among the fire-related factors in a SEM (the rationale of the proposed relationships is described in the Materials and Methods). The hypothesized causal model outperformed the model validity analysis ( $p\text{-value}>0.05$  in the chi-squared test; details on the covariances and residuals in the model are shown in Table S2). The SEM supported the role of temperature in controlling other factors that affect the extent of burning (Fig. 5 and Fig. S8). Temperature showed significant positive relationships with the lengthening of the growing season (0.66), the vegetation green biomass represented by  $\text{NDVI}_{\text{mean}}$  (0.60), and atmospheric dryness measured by VPD (0.93). We hypothesized that these temperature-regulated factors and total precipitation would influence plant water stress, measured by climatic water deficit, but only VPD showed a significant effect (0.75) for the low number of observations ( $n = 20$ ). Despite this, the hypothesized relationships displayed the expected sign. Temperature and CWD had a positive relationship with the number of detected ignitions (0.49 and 0.43, respectively). Annual burned area presented a  $R^2$  of 0.82 and was directly explained by the number of detected ignitions (0.48) and the CWD (0.46).

Climate factors may differ locally and throughout the fire season. An additional analysis based on local weather conditions during the burning revealed that ignitions affecting areas larger than 4,000 ha occurred with average hourly maximum temperatures of  $28.6^{\circ}\text{C}$  ( $\text{sd} = 3.4^{\circ}\text{C}$ ) and mean wind direction from the North-East (Fig. S9). 30-day pre-ignition precipitation was 0.37 mm ( $\text{sd} = 0.81\text{ mm}$ ), and mean wind speed was  $0.96\text{ m s}^{-1}$  ( $\text{sd} = 0.55\text{ m s}^{-1}$ ). Ignitions that burn areas larger than 4,000 ha only represent 10% of all counts, but account for 81% of all burned areas that were mapped between 2001 and 2020.

### ***Projections of annual burned area and carbon emissions under warming scenarios***

Annual burned area in 2018, 2019, and 2020 more than doubled the long-term average, which was 0.24 Mha for the period 1982-2020 in the Siberian Arctic. Summer 2001, with a mean temperature nearing  $10^{\circ}\text{C}$ , was the first year on record to have a mapped burned area over twice that of the long-term average. The exponential regression between the burned area and temperature (Fig. 4) indicated that an annual burn of 0.5 Mha occurred at a mean summer temperature of  $10.2^{\circ}\text{C}$ . The  $10^{\circ}\text{C}$  threshold also indicated the rapid growth of the annual burned area in 2018, 2019, and 2020. This indicates that small increases in summer mean temperature above the  $10^{\circ}\text{C}$  threshold tend to be associated with extensive annual burned areas.

The linear trend of mean summer air temperature (Fig. 3) indicated that temperatures would reach  $10.2^{\circ}\text{C}$  by 2024 and reach the levels in 2020 by 2045 if mean summer temperatures continued to increase linearly at the current rate. (Fig. 6a). The RCP 4.5 and 8.5 scenarios also indicated an increase in temperatures that could substantially expand the burned area in the

Siberian Arctic; annual burned area could range from 0.5 to 2.5 Mha before the middle of the century under RCP 4.5 and RCP 8.5 (Fig. 6b). This would result in a mean annual emission of 37.8 (sd = 14.4) Tg C y<sup>-1</sup> and 107.0 (sd = 40.7) Tg CO<sub>2</sub>-eq y<sup>-1</sup> under RCP 8.5 between 2030 and 2050 (Fig. 6c), of which 27.6% would come from carbon-rich peatlands (Fig. 6d). Large fires of the magnitude observed in 2020 (burned area > 2.5 Mha) would become more frequent in the second half of the century under RCP 8.5, with a return interval lower than 2 years and annual mean carbon emissions of 135.0 (sd = 69.0) Tg C y<sup>-1</sup> and 382.5 (sd = 195.6) Tg CO<sub>2</sub>-eq y<sup>-1</sup> (27.9% from carbon-rich peatlands). Under the RCP 4.5 scenario, annual carbon emissions would stabilize (51.7 (sd = 18.8) Tg C y<sup>-1</sup>) in the second half of the century, and fires such as those in 2020 would become less frequent, with a 5-year return interval if carbon emissions stabilize by mid-century.

## Discussion

The Siberian Arctic burned at the highest rates in 2019 and 2020, based on the burning trends over four decades of satellite data. Burning was seven-fold higher in 2020 than the 1982-2020 average and damaged an unprecedented area of peatlands. We found that temperature-related factors of fire regime have increased significantly over the last four decades and identified an exponential relationship between these factors and annual burned area, accounting for the unprecedented extent of the burns in 2019 and 2020.

The SEM results confirmed the positive association between higher temperatures, longer growing season and greener vegetation. Higher temperatures account for the earlier snowmelt, permitting vegetation growth (17) and increased green biomass (18), which increases fuel availability. This earlier start of the growing season, also reported more widely (19), modifies water use and availability such that plants may also experience water stress earlier in the season (20). According to the SEM results, the length of season and increasing green biomass of vegetation were associated with increased plant water stress, but the association was not significant, likely due to the limited number of observations.

The increasing vulnerability to drought is exacerbated by extreme heatwaves, as in 2020, which can potentially desiccate plants and reduce moisture in peat, and thus increase severity of burning (21). This is reflected by the high influence of atmospheric dryness, measured by VPD, on plant water stress, represented by CWD, and its high correlation with annual burned area. Furthermore, CWD encompasses climatic factors, the water balance, and phenological changes that influence the susceptibility of vegetation to fire, so the interconnection of the fire factors with CWD may explain why CWD was best correlated with the annual burned area.

Climate warming and extreme weather may also account for the increase in the number of ignitions for specific years. The year 2020 had record-breaking temperatures and caused drought conditions early during the growing season (13). Recent warm winters, such as 2020, appear associated with abnormal circulation patterns that also favor the early spring snow melt and lower albedo that maintain warm conditions (22). Heatwaves and, more especially, increased surface temperatures are associated with convective storms and lightning, as confirmed with the SEM. While lightning remains infrequent at high latitudes, it is expected to increase as the climate warms (23). Climatic warming thus has a dual effect on fire regimes; warming increases the susceptibility of vegetation and peatlands to fire and increases the number of lightning-caused ignitions.



Increased winter warmth, as seen in 2020, reflects changes in circulation that draw more heat and moisture from lower latitudes (24). Circulation in Eastern Siberia draws air and moisture from all directions of the compass (25) and is not immune to the so called circulation “blocking” (26) seen elsewhere across the continent (27). Nonetheless, most burning occurs during relatively gentle winds blowing from the North-East, indicating the processes promote flammability may be distinct from those that promote the subsequent burning.

Our ignition detection method indicated that numerous fires started near simultaneously across a vast region during a period of atmospheric instability in the 2020 fire season, from which we speculate that lightning was the main cause of ignition, but local observations are required to verify this supposition. An alternative, or additional, explanation is that fires emerge from smoldering material that has persisted through the winter to re-emerge when conditions permit a broader conflagration (28, 29). We also found that satellite thermal sensors showed that fires spread quickly after high CAPE values and mid-season ignitions, which suggests that most of the annual burned area is caused by fires that start during that time.

The link we see between fires and temperature suggests that severe fire years, like 2020, will become increasingly common and resulting carbon emissions will rise. The magnitude of these fires and carbon emissions, however, remains uncertain. First, while the frequency of lightning strikes appears likely to increase as temperatures rise (23), the scale of any resulting fires depends on specific local weather and vegetation conditions, which remain challenging to predict. Second, we only considered direct emissions from burning and disregarded indirect emissions, though these are not necessarily negligible. Burning removes the peat that insulates permafrost, exposing it to thawing, which promotes soil respiration and the production of carbon dioxide and methane (30). Estimates from field studies in two different boreal forests in Alaska suggest that post-fire carbon emissions range from one third to more than double those that occur during burning (31). Furthermore, permafrost prevents deeper burning in peatlands (21). As permafrost retreats, high temperatures and drying conditions may favour higher combustion rates (32). We used combustion rates ranging from 2.0 kg C m<sup>-2</sup> for tundra to 3.4 kg C m<sup>-2</sup> for boreal forests (31), but dry peatlands can release up to 16.8 kg C m<sup>-2</sup> (21), indicating that much higher emissions are credible.

A previous study proposed temperature and rainfall thresholds for the annual burned areas in the Alaskan tundra (15). The extensive area burned in 2019 and 2020 corroborated the proposed curve-growth relationship between annual burned area and climate-related factors for the Alaskan tundra. Hu et al. (15) forecasted that the annual burned area would double in the Alaskan tundra by the end of the century. We found, however, that the annual burned area in the Siberian Arctic already doubled the long-term average in the last three years of the record. This increase in annual burned area suggests that the Arctic is already experiencing a change in fire regimes caused by climatic warming. The burned areas in 2019 and 2020 might be exceptional occurrences, but the recent temperature trend and projected scenarios indicate that temperatures are reaching a threshold in which small increases above 10 °C can alter fire-related factors and result in exponentially increasing burned area and associated fire emissions in the next decades. Forthcoming fires can potentially affect peatlands and deteriorate the permafrost, which in turn will exacerbate the carbon emissions from carbon-rich soils.

## References and Notes

1. S. M. Natali, J. P. Holdren, B. M. Rogers, R. Treharne, P. B. Duffy, R. Pomerance, E. MacDonald, Permafrost carbon feedbacks threaten global climate goals. *Proceedings of the National Academy of Sciences*. **118** (2021).
- 5 2. M. C. Serreze, J. A. Francis, The Arctic amplification debate. *Climatic change*. **76**, 241–264 (2006).
3. E. Post, The polar regions in a 2 C warmer world. *Science advances*. **5** (2019).
4. AMAP, Arctic Climate Change Update 2021: Key Trends and Impacts. Summary for Policy-Makers (2021).
- 10 5. E. A. Schuur, A. D. McGuire, C. Schädel, G. Grosse, J. W. Harden, D. J. Hayes, G. Hugelius, C. D. Koven, P. Kuhry, D. M. Lawrence, others, Climate change and the permafrost carbon feedback. *Nature*. **520**, 171–179 (2015).
6. K. Dutta, E. Schuur, J. Neff, S. Zimov, Potential carbon release from permafrost soils of Northeastern Siberia. *Global Change Biology*. **12**, 2336–2351 (2006).
- 15 7. M. R. Turetsky, B. W. Abbott, M. C. Jones, K. W. Anthony, D. Olefeldt, E. A. Schuur, G. Grosse, P. Kuhry, G. Hugelius, C. Koven, others, Carbon release through abrupt permafrost thaw. *Nature Geoscience*. **13**, 138–143 (2020).
8. G. Hugelius, J. Loisel, S. Chadburn, R. B. Jackson, M. Jones, G. MacDonald, M. Marushchak, D. Olefeldt, M. Packalen, M. B. Siewert, others, Large stocks of peatland carbon and nitrogen are vulnerable to permafrost thaw. *Proceedings of the National Academy of Sciences*. **117**, 20438–20446 (2020).
- 20 9. A. Witze, The Arctic is burning like never before—and that’s bad news for climate change. *Nature*. **585**, 336–337 (2020).
10. M. C. Mack, M. S. Bret-Harte, T. N. Hollingsworth, R. R. Jandt, E. A. Schuur, G. R. Shaver, D. L. Verbyla, Carbon loss from an unprecedented Arctic tundra wildfire. *Nature*. **475**, 489–492 (2011).
- 25 11. N. H. French, L. K. Jenkins, T. V. Loboda, M. Flannigan, R. Jandt, L. L. Bourgeau-Chavez, M. Whitley, Fire in arctic tundra of Alaska: past fire activity, future fire potential, and significance for land management and ecology. *International Journal of Wildland Fire*. **24**, 1045–1061 (2015).
- 30 12. J. L. McCarty, J. Aalto, V.-V. Paunu, S. R. Arnold, S. Eckhardt, Z. Klimont, J. J. Fain, N. Evangelizou, A. Venäläinen, N. M. Tchebakova, others, Reviews and syntheses: Arctic fire regimes and emissions in the 21st century. *Biogeosciences*. **18**, 5053–5083 (2021).
- 35 13. A. Ciavarella, D. Cotterill, P. Stott, S. Kew, S. Philip, G. J. van Oldenborgh, A. Skålevåg, P. Lorenz, Y. Robin, F. Otto, others, Prolonged Siberian heat of 2020 almost impossible without human influence. *Climatic Change*. **166**, 1–18 (2021).



14. O. V. Churakova Sidorova, R. T. Siegwolf, M. V. Fonti, E. A. Vaganov, M. Saurer, Spring arctic oscillation as a trigger of summer drought in Siberian subarctic over the past 1494 years. *Scientific reports*. **11**, 1–10 (2021).
- 5 15. F. S. Hu, P. E. Higuera, P. Duffy, M. L. Chipman, A. V. Rocha, A. M. Young, R. Kelly, M. C. Dietze, Arctic tundra fires: natural variability and responses to climate change. *Frontiers in Ecology and the Environment*. **13**, 369–377 (2015).
16. P. Olofsson, G. M. Foody, M. Herold, S. V. Stehman, C. E. Woodcock, M. A. Wulder, Good practices for estimating area and assessing accuracy of land change. *Remote Sensing of Environment*. **148**, 42–57 (2014).
- 10 17. A. Descals, A. Verger, I. Filella, D. Baldocchi, I. A. Janssens, Y. H. Fu, S. Piao, M. Peaucelle, P. Ciais, J. Peñuelas, Soil thawing regulates the spring growth onset in tundra and alpine biomes. *Science of the Total Environment*. **742**, 140637 (2020).
18. L. T. Berner, R. Massey, P. Jantz, B. C. Forbes, M. Macias-Fauria, I. Myers-Smith, T. Kumpula, G. Gauthier, L. Andreu-Hayles, B. V. Gaglioti, others, Summer warming explains widespread but not uniform greening in the Arctic tundra biome. *Nature communications*. **11**, 1–12 (2020).
- 15 19. S. Piao, Q. Liu, A. Chen, I. A. Janssens, Y. Fu, J. Dai, L. Liu, X. Lian, M. Shen, X. Zhu, Plant phenology and global climate change: Current progresses and challenges. *Global change biology*. **25**, 1922–1940 (2019).
- 20 20. J. Peñuelas, T. Rutishauser, I. Filella, Phenology feedbacks on climate change. *Science*. **324**, 887–888 (2009).
21. M. Turetsky, Wf. Donahue, B. Benscoter, Experimental drying intensifies burning and carbon losses in a northern peatland. *Nature Communications*. **2**, 1–5 (2011).
- 25 22. A. B. M. Collow, N. P. Thomas, M. G. Bosilovich, Y.-K. Lim, S. D. Schubert, R. D. Koster, Seasonal variability in the mechanisms behind the 2020 Siberian heatwaves. *Journal of Climate*. **35**, 3075–3090 (2022).
23. Y. Chen, D. M. Romps, J. T. Seeley, S. Veraverbeke, W. J. Riley, Z. A. Mekonnen, J. T. Randerson, Future increases in Arctic lightning and fire risk for permafrost carbon. *Nature Climate Change*. **11**, 404–410 (2021).
- 30 24. Q. You, Z. Cai, N. Pepin, D. Chen, B. Ahrens, Z. Jiang, F. Wu, S. Kang, R. Zhang, T. Wu, others, Warming amplification over the Arctic Pole and Third Pole: Trends, mechanisms and consequences. *Earth-Science Reviews*. **217**, 103625 (2021).
25. J. Piao, W. Chen, S. Chen, H. Gong, Q. Zhang, Summer water vapor sources in Northeast Asia and East Siberia revealed by a moisture-tracing atmospheric model. *Journal of Climate*. **33**, 3883–3899 (2020).
- 35 26. C. You, M. Tjernström, A. Devasthale, D. Steinfeld, *Geophysical Research Letters*, in press.

27. T. Nakamura, T. Sato, A possible linkage of Eurasian heat wave and East Asian heavy rainfall in Relation to the Rapid Arctic warming. *Environmental Research*. **209**, 112881 (2022).
28. R. C. Scholten, R. Jandt, E. A. Miller, B. M. Rogers, S. Veraverbeke, Overwintering fires in boreal forests. *Nature*. **593**, 399–404 (2021).
29. J. L. McCarty, T. E. Smith, M. R. Turetsky, Arctic fires re-emerging. *Nature Geoscience*. **13**, 658–660 (2020).
30. J. E. Holloway, A. G. Lewkowicz, T. A. Douglas, X. Li, M. R. Turetsky, J. L. Baltzer, H. Jin, Impact of wildfire on permafrost landscapes: A review of recent advances and future prospects. *Permafrost and Periglacial Processes*. **31**, 371–382 (2020).
31. S. Veraverbeke, C. J. Delcourt, E. Kukavskaya, M. Mack, X. Walker, T. Hessilt, B. Rogers, R. C. Scholten, Direct and longer-term carbon emissions from arctic-boreal fires: A short review of recent advances. *Current Opinion in Environmental Science & Health*. **23**, 100277 (2021).
32. M. R. Turetsky, B. Benscoter, S. Page, G. Rein, G. R. Van Der Werf, A. Watts, Global vulnerability of peatlands to fire and carbon loss. *Nature Geoscience*. **8**, 11–14 (2015).
33. A. Descals, Z. Szantoi, E. Meijaard, H. Sutikno, G. Rindanata, S. Wich, Oil palm (*Elaeis guineensis*) mapping with details: Smallholder versus industrial plantations and their extent in Riau, Sumatra. *Remote Sensing*. **11**, 2590 (2019).

**Acknowledgments:** Acknowledgments follow the references and notes list but are not numbered. Start with text that acknowledges non-author contributions and then complete each of the sections below as separate paragraphs.

**Funding:** This work was funded by the Ministry of Agriculture, Forestry and Fisheries (MAFF) of the government of Japan and the Center for International Forestry Research (“CIFOR”), through the project “Transitions to Climate Resilient Landscapes: Reducing and Mitigating Boreal and Tropical Forest Fires to Promote Sustainable Rural Livelihoods”. We acknowledge funds from the Spanish Government grant PID2019-110521GB-I00, the Fundación Ramón Areces grant ELEMENTAL-CLIMATE, the Catalan Government grant SGR 2017-1005.

**Author contributions:**

Conceptualization: AD, DG, JP

Methodology: AD, DG

Investigation: AD, DG

Visualization: AD, DG, JP

Supervision: JP

Writing – original draft: AD, DG

Writing – review & editing: AD, DG, AV, DS, DN, JP

**Competing interests:** Authors declare that they have no competing interests.

**Data and materials availability:** All source code and the Sentinel-2 and Landsat-8 burned area maps produced in this study are available at Zenodo (33). Other data that support the findings of the study are openly available. The burned area time series derived from AVHRR sensors (FireCCILT11) is available at [\[http://dx.doi.org/10.5285/62866635ab074e07b93f17fbf87a2c1a\]](http://dx.doi.org/10.5285/62866635ab074e07b93f17fbf87a2c1a). The burned area time series derived from MODIS sensors are available at [\[https://doi.org/10.5067/MODIS/MCD64A1.006\]](https://doi.org/10.5067/MODIS/MCD64A1.006) for the MCD64A1 product and [\[https://doi.org/10.5285/58f00d8814064b79a0c49662ad3af537\]](https://doi.org/10.5285/58f00d8814064b79a0c49662ad3af537) for the FireCCI51 product. The burned area time series derived from Sentinel-3 (C3SBA10) is available at [\[https://doi.org/10.24381/cds.f333cf85\]](https://doi.org/10.24381/cds.f333cf85). The Landsat-7 and -8 surface reflectance datasets are available at [\[https://earthexplorer.usgs.gov\]](https://earthexplorer.usgs.gov), and the Sentinel-2 Level-2A surface reflectance at [\[https://scihub.copernicus.eu\]](https://scihub.copernicus.eu). The active fire datasets obtained from MODIS is available at [\[https://firms.modaps.eosdis.nasa.gov/active\\_fire\]](https://firms.modaps.eosdis.nasa.gov/active_fire). Fire emission datasets were downloaded from the FIRECAM platform [\[https://globalfires.earthengine.app/view/firecam/\]](https://globalfires.earthengine.app/view/firecam/). Land surface temperature from MODIS (MOD11A2) is available at [\[https://doi.org/10.5067/MODIS/MOD11A2.006\]](https://doi.org/10.5067/MODIS/MOD11A2.006). Time series of temperature, total precipitation, vapor-pressure deficit, and components of the wind speed from the ERA5-Land Monthly are available at [\[https://doi.org/10.24381/cds.68d2bb30\]](https://doi.org/10.24381/cds.68d2bb30), and the climatic water deficit from the TERRACLIMATE dataset is available at [\[https://doi.org/10.7923/G43J3B0R\]](https://doi.org/10.7923/G43J3B0R). The downscaled air temperature from the HadGEM2-CC model is available at [\[https://doi.org/10.24381/cds.a37fecb7\]](https://doi.org/10.24381/cds.a37fecb7). The storage of organic carbon from peatlands is available at [\[https://bolin.su.se/data/hugelius-2020\]](https://bolin.su.se/data/hugelius-2020). Lastly, the NDVI time series from the GIMMS3g dataset is available at [\[https://www.nasa.gov/nex/data\]](https://www.nasa.gov/nex/data), and the NDVI from the MOD13Q1v6 product at [\[https://doi.org/10.5067/MODIS/MOD13Q1.006\]](https://doi.org/10.5067/MODIS/MOD13Q1.006).

## Supplementary Materials

Materials and Methods

Supplementary Text

References (34-57)

Figs. S1 to S9

Tables S1 and S2

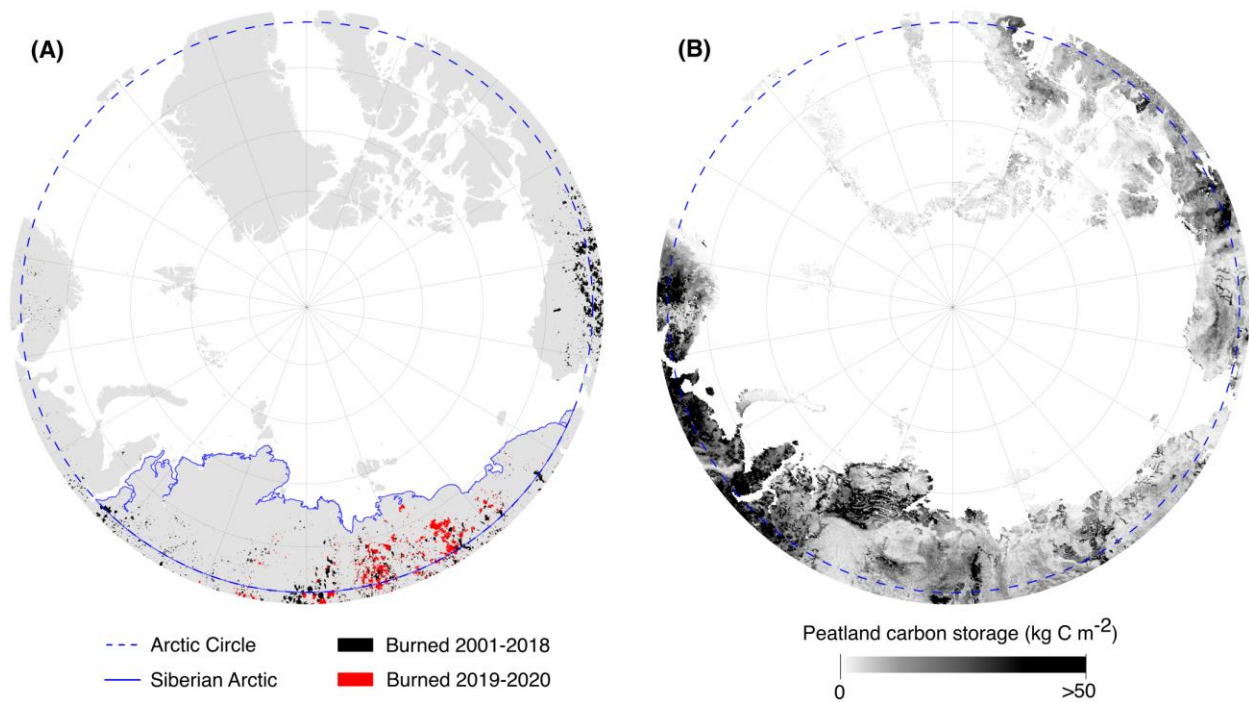


**Fig. 1. Maps of burned area for 2001-2020 and peatland carbon storage in the circumpolar region.** (A) the extents of the burns for 2001-2018 are from the FireCCI51 product, and the extents for 2019 and 2020 are the union of the C3SBA10 product and the Sentinel-2 burned area map developed in this study. The Siberian Arctic is the area inside the blue outline. Black represents areas that burned at least once for 2001-2018, and red represents areas that burned in 2019 and 2020. Areas that burned at least once in both periods, in 2001-2018 and 2019-2020, are also depicted in red color; these areas represent only 3% of total burning above the Arctic Circle during the 2001-2020 period. We show the annual burned area from 2001 to 2020, which is the period when the occurrence of fires accelerated. (B) Estimated storage of organic carbon in peatlands from a reference dataset (8).

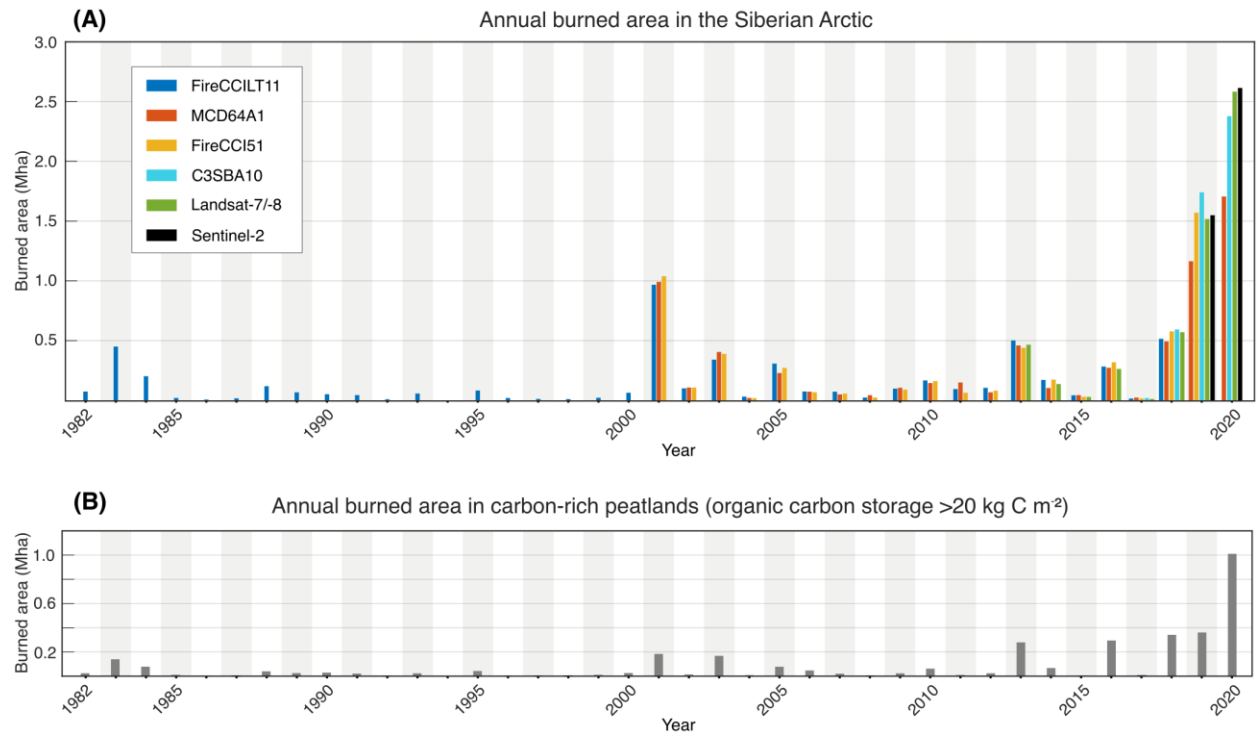


**Fig. 2. Annual burned area in the Siberian Arctic and in carbon-rich peatlands for 1982-2020.** (A) Annual burned area in the Siberian Arctic derived from remotely sensed data from six products. (B) Annual burned area in carbon-rich peatlands;  $>20 \text{ kg C m}^{-2}$  in storage of organic carbon obtained from a reference dataset (8). The annual burned area in carbon-rich peatlands represent the median burned area for the available satellite products. Year 1994 contains no data.

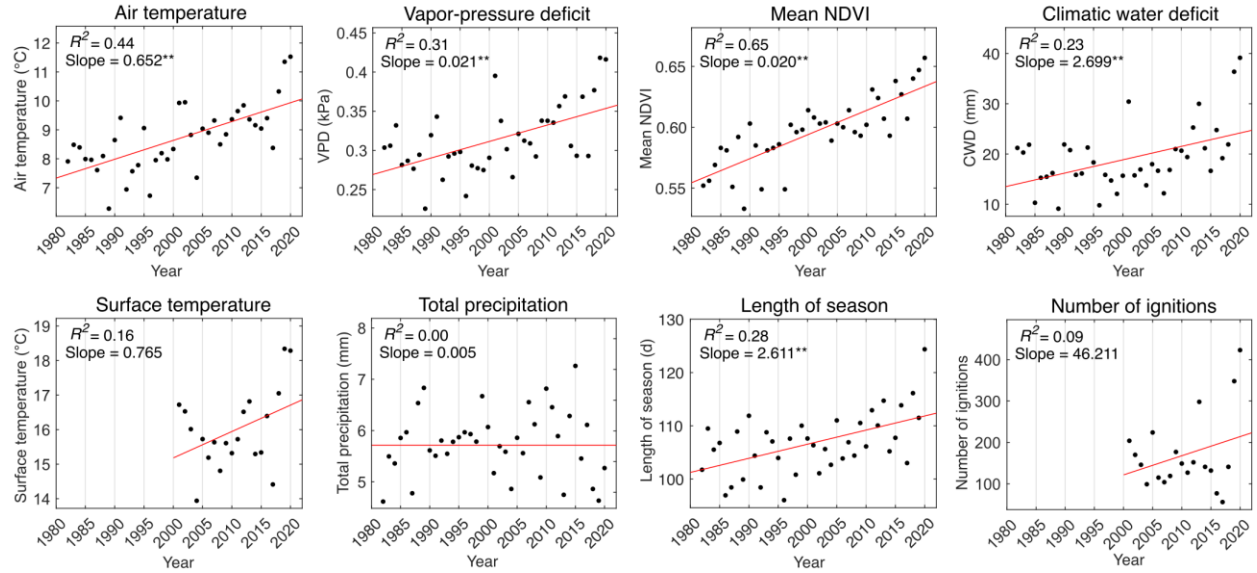


**Fig. 3. Trends of eight fire factors in the Siberian Arctic during 1982-2020.** The factors are the mean summer air and surface temperature, mean vapor-pressure deficit (VPD), total summer precipitation, mean climatic water deficit (CWD), mean normalized difference vegetation index (NDVI) depicting vegetation green biomass, the length of the growing season, and the number of detected ignitions. The red lines are linear regressions; slopes are estimated on a decadal time scale (\*,  $p < 0.05$ ; \*\*,  $p < 0.01$ ).



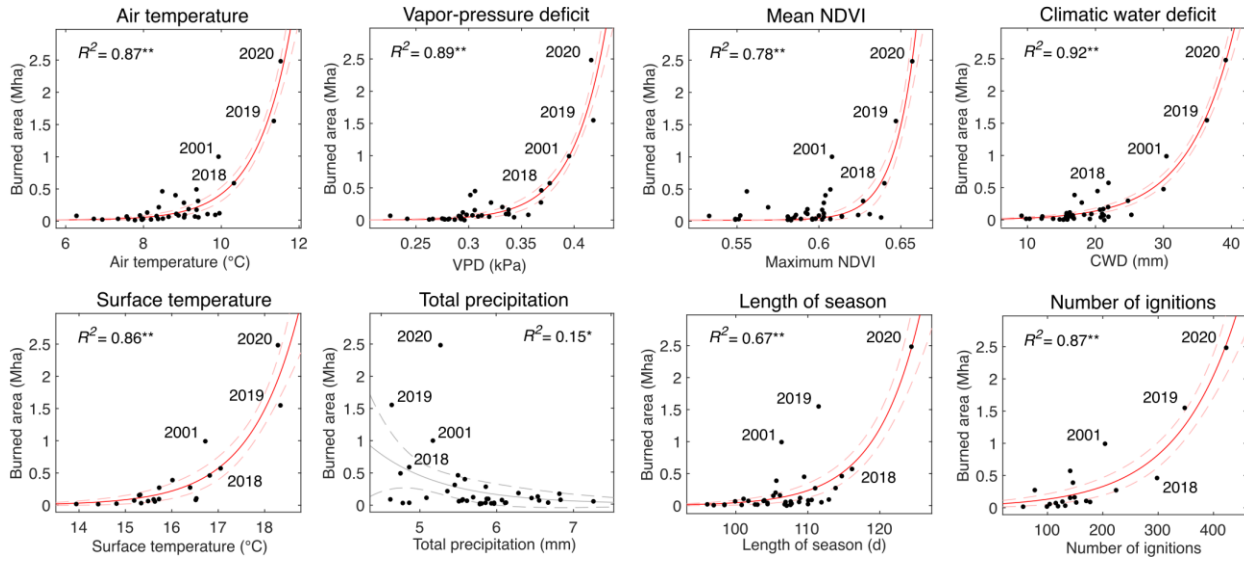


**Fig. 4. Regression between the annual burned area and eight fire factors in the Siberian Arctic during 1982-2020.** The solid lines are the best regression (linear or exponential) based on the coefficient of determination ( $R^2$ ; \*,  $p < 0.05$ ; \*\*,  $p < 0.01$ ). The best regression model was the exponential for all the factors. The annual burned area is the median burned area for the available satellite products. The factors are the mean summer air and surface temperature, mean vapor-pressure deficit (VPD), total precipitation, mean climatic water deficit (CWD), mean normalized difference vegetation index (NDVI) depicting green biomass, the start of the growing season, and the number of ignitions. Red solid lines depict a fit with a significant correlation ( $p < 0.05$ ). The dashed lines are the 95% prediction limits of the regressions.

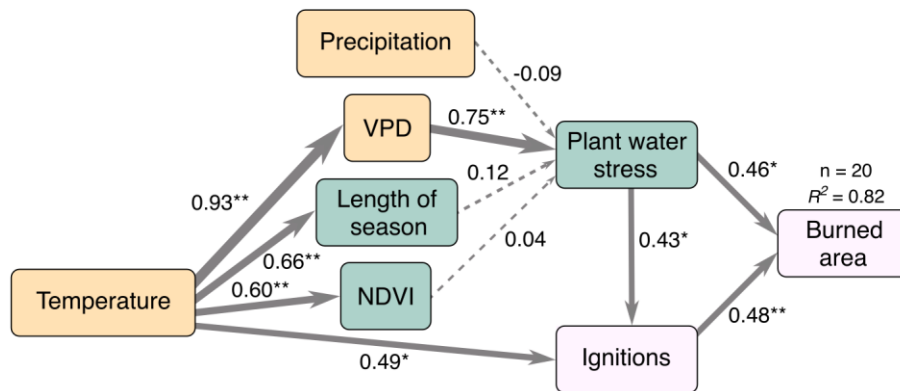


**Fig. 5. Causality networks for the association among factors of fire in the Siberian Arctic for 2001-2020.** The variables are categorized as climate-variables in yellow (mean summer surface temperature, total precipitation, mean vapor-pressure deficit (VPD)), vegetation-variables in green (mean summer normalized difference vegetation index (NDVI) depicting green biomass, the length of the growing season, plant water stress measured by mean summer climatic water deficit (CWD)), and fire-variables in light red (number of detected ignitions and annual burned area). Factor loadings between variables are shown next to lines (\*,  $p < 0.05$ ; \*\*,  $p < 0.01$ ). The width of the lines depicts the magnitude of the effect and dashed lines represent non-significant effects.  $R^2$  is the variance explained for the annual burned area.

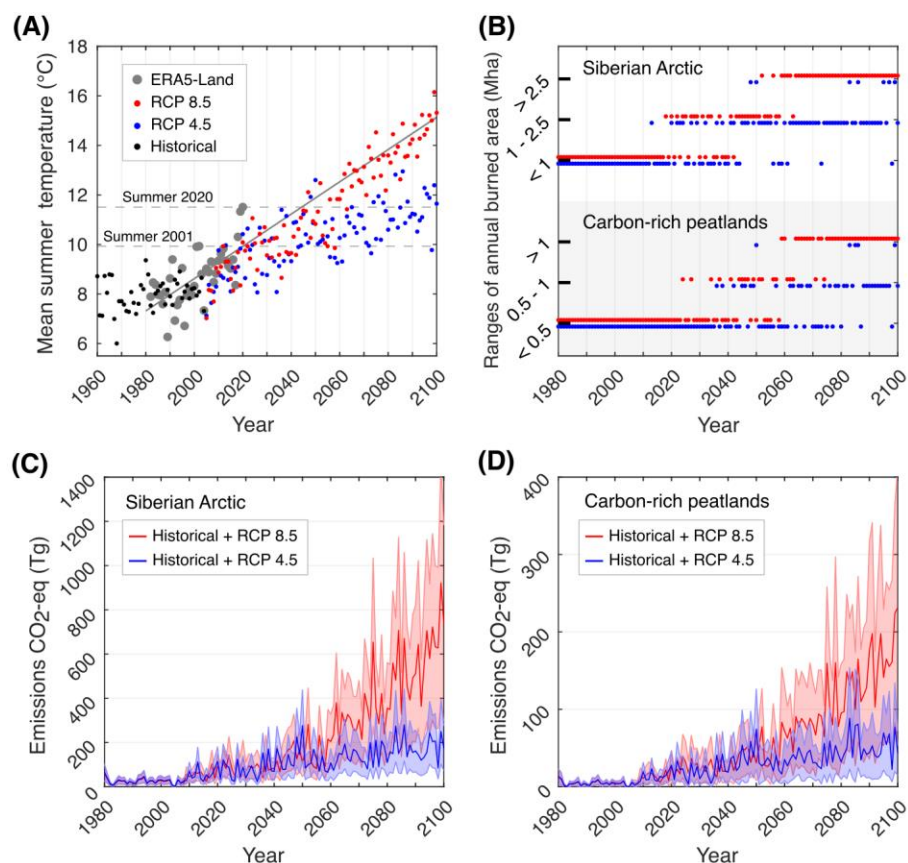


**Fig. 6. Projected temperatures, annual burned areas (BA), and emissions from fire in the Siberian Arctic.** (A) Mean summer air temperatures from climate reanalysis (ERA-5 Land) during 1982–2020, and historical and projected temperatures under the RCP 4.5 and 8.5 scenarios based on HadGEM2-CC model. (B) Ranges of annual burned areas for the historical period and under the RCP 4.5 and 8.5 scenarios for the entire Siberian Arctic and only considering carbon-rich peatlands (organic carbon storage  $>20 \text{ kg C m}^{-2}$ ). The lower and upper thresholds of the ranges are approximately the annual burned areas in 2001 and 2020, respectively. Projected CO<sub>2</sub>-eq emissions under the RCP 4.5 and 8.5 in (C) Siberian Arctic and (D) carbon-rich soils.